1998

Finite element analysis of chip formation in grooved tool metal cutting

Wooi Khiong Thean
Iowa State University

Finite element analysis of chip formation

in grooved tool metal cutting

by

Wooi Khiong Thean

A thesis submitted to the graduate faculty

in partial fulfillment of the requirements for the degree of

MASTER OF SCIENCE

Major: Mechanical Engineering

Major Professor: G. Ivan Maldonado

Iowa State University

Ames, Iowa

1998

Graduate College
Iowa State University

This is to certify that the Master's thesis of

Wooi Khiong Thean

has met the thesis requirements of Iowa State University

Signatures have been redacted for privacy

TABLE OF CONTENTS

LIST OF FIGURES

ACKNOWLEDGMENTS

The successful completion of my work would not be possible without the help and support of many people. Thank you to all of you and especially to the following individuals. I would like to thank my major professor Dr. Ivan Maldonado for his invaluable help and guidance. Although often occupied by the "one-million-things-waiting-for-me-to-do", his patience and willingness to encourage and guide me in my research are most appreciated. Thanks also to Dr. Daniel Fang and Dr. Ranga Narayanaswami for their helpful suggestions in my research and also for reviewing my thesis. My appreciation also goes to Dr. Thomas Rogge for his advice on the finite element aspect of this work. I would like to thank Dr. Judy Vance for generously sponsoring me to use the computer facilities in the Iowa Center for Emerging Manufacturing Technology (ICEMT). I am also grateful to Patrick Bergan of ICEMT and John Minor of Black Engineering for helping me with the computer problems that I encountered in my research. Thanks also to Rosalie Enfield of Black Engineering for helping me to keep track and take care of all the paper work that I needed to complete my degree. And to Lena, thank you so much for your support. Your joyous and gracious smiles have always cheered me up. Most of all, I would like to thank my two great parents. Their love and encouragement have always kept me going through all the good and bad times.

1 INTRODUCTION

Machining is one of the most widely used operations in industry today. It is a material removal process which can be the traditional metal cutting, an abrasive process such as grinding, or entail nontraditional processes such as electrochemical and laser machining. Among these, metal cutting is the most popular with manufacturers because it facilitates the production of large volumes of complex parts with unprecedented dimensional accuracy and in a relatively short time. In addition, metal cutting enables manufacturers to mass produce identical parts cheaply, and this process is also applicable to other non-metallic materials such as polymers, wood and ceramics.

Although metal cutting has been widely researched since the 1900's, the selection of cutting parameters such as tool materials, tool geometries, cutting speeds, feed rates and depths of cut for low production volumes is still based on machinist experience or handbook recommendations. The selected parameters are seldom optimum, but low production volumes do not justify tests to increase efficiency. For high production volumes, the cutting parameters are obtained from tests which pursue maximum efficiency, and the cost of testing is offset by the large quantity of parts produced. In either case, machining tests are expensive and time consuming. Thus, the need exists to either develop more efficient strategies that minimize the number of tests, or to eliminate testing completely.

1.1 The Mechanics of Cutting Process

The mechanics of metal cutting is still not clearly understood because the physics of the cutting process are extremely complex. Moreover, studies performed on one set of tool-workpiece combination may not be extended to another set due to different material properties. Minimal changes in the material properties of the tool or workpiece dictate significant changes in the type of chips formed, thus affecting the resulting cutting forces, feed rate or cutting speed.

To study the mechanics of metal cutting in a manageable perspective, a simplified model can be assumed. In traditional metal cutting processes, metal is removed as a plastically deformed chip. Hence, a fairly unified physical analysis of the cutting mechanics can be studied by looking at the chip

formation process. Although the chip has no commercial value, the mechanics of chip formation can help quantify such parameters as cutting power, tool temperatures and cutting forces which influence machining accuracy and tool life.

A common analytical model used to describe the cutting process is the orthogonal cutting model shown in Figure 1.1. The edge of the wedge-shaped tool is perpendicular to the cutting direction. The tool is assumed to be rigid and stationary, and the workpiece is assumed to move towards the tool with a constant velocity. As the tool cuts into the material, a continuous plastically deformed chip is formed through a shearing process in the primary shear zone. Further plastic deformation takes place in the secondary shear zone at the tool-chip interface, due to adhesion and frictional sliding as demonstrated by Trent [1]. The newly formed workpiece surface does not come in contact with the tool flank face because of the clearance angle. In orthogonal cuting, the workpiece material is considered to be under plane strain conditions since the chip width is much greater than its thickness. All these conditions form the basis for the analysis of two-dimensional steady state cutting that produces a continuous chip.

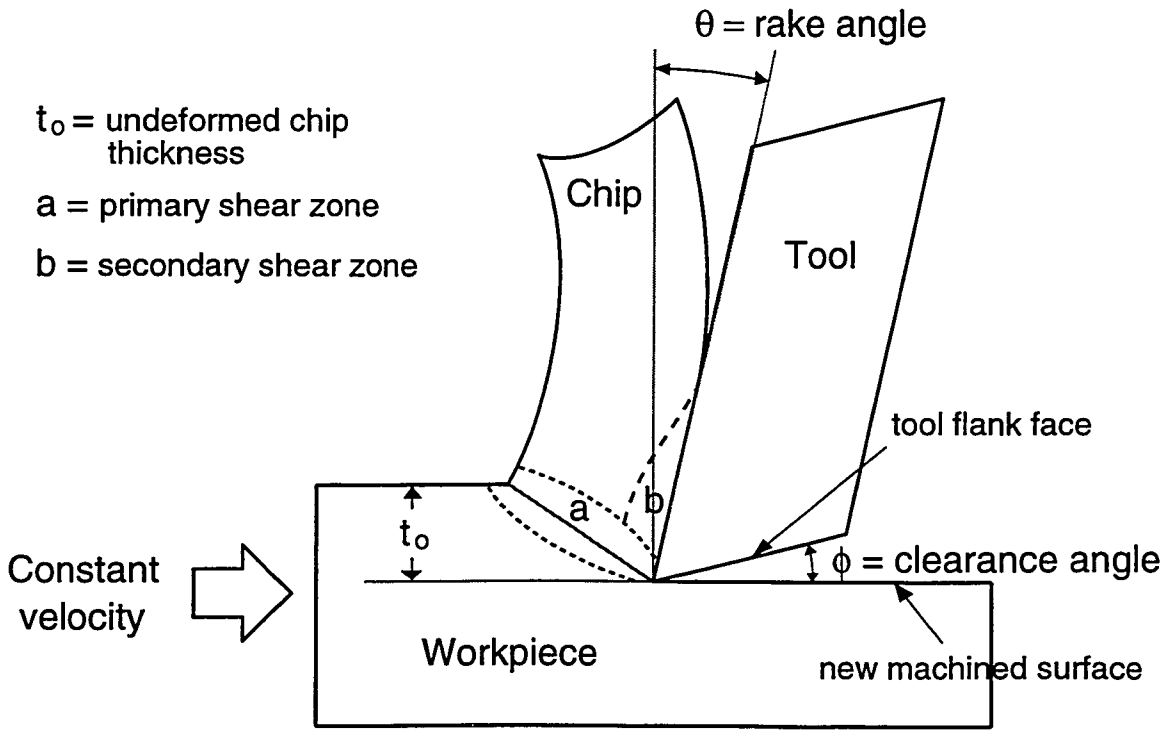

Figure 1.1 Simplified orthogonal cutting model

The types of chip formed depend on the combination of tool and workpiece material as well as the cutting parameters such as rake angle, depth of cut and cutting speed. The most desirable type of chip is the continuous chip without any built-up edge. This type of chip is formed when ductile materials are machined at high speeds with small feed and shallow depth of cut. It results in good surface finish and the most accurate dimensions. Thus, most metal cutting studies are modeled with continuous chip formation, where the relation between the cutting parameters and the behavior of the chip is analyzed.

1.2 The Finite Element Method

The finite element method (FEM) is used extensively today in many engineering analysis from structural and solid mechanics to field problems such as heat transfer and fluid flow problems. The essence of FEM seeks to solve systems of differential equations which govern a physical model, a task which is typically more practical and feasible with the use of digital computers. With the advances in computer technology, FEM continues to see a wide-spread use and is increasingly becoming an integral part of engineering analysis.

The use of FEM in metal cutting analyses has several advantages. First, FEM analysis enables one to estimate many properties of the tool and chip materials which cannot be easily obtained from experimental data. Traditionally, strain and stress contours can be obtained from cutting experiments using imprinted grid and photo-elastic materials. These methods, however, are limited to certain tool-workpiece material combinations and to low speed cutting. Also, other properties like the principal stress, maximum shear stress and maximum shear strain need to be calculated thus, contours of these properties are difficult to generate from the experimental data. Alternatively, most modern FEM codes provide the convenience of displaying these contours via numerical calculations performed by a computer.

Moreover, FEM can be used to minimize the number of tests needed to fine-tune the parameters for optimum cutting conditions. Typically, empirical equations derived from actual experiments have been the source for obtaining these parameters. Experiments, however, are cumbersome and time consuming, and the data collected for specific tool-work material combinations is useful for only a limited cutting range. With FEM, the tool-work material properties are specified beforehand and the cutting parameters can be easily changed to analyze the impact. Simulations can be performed until the optimum cutting parameters are obtained, and then verified by actual tests.

There are two traditional ways of formulating FEM simulations in metal cutting; the updated Lagrangian formulation and the Eulerian formulation. Most metal cutting simulations were performed

on the updated Lagrangian formulation. In this formulation, the time variable is used as a convenient way to describe the loading and motion of a body. The aim is to evaluate the equilibrium position of the complete body at each of the discrete time points. After each time step evaluation, the body is updated from its previous equilibrium position to a new equilibrium position. The final result is obtained when the final configuration of the body is solved for the final time step. In other words, all the particles in the body of interest are followed through from one configuration to another. The advantage of this formulation is that the shape of the chip does not need to be assumed. The formulation allows the prescription of a predefined parting line, and a failure criterion for the chip to separate from the workpiece. Thus, the predefined chip segment could separate and its position solved at each time step, allowing the actual simulation of the chip formation process from incipient cutting to steady state cutting.

In the Lagrangian formulation, large deformation in the finite element mesh can cause convergence problems. In contrast, the Eulerian formulation can handle large deformation because the mesh acts as a stationary control volume, and the analysis is focused on the material that moves through this volume. This is made possible by prescribing a viscous behavior in the workpiece material. Another advantage of this formulation is a reduced computational effort in the overall analysis because a finer element mesh can be confined to the shear zone area where the largest deformation occurs. Also, node separation calculations are not required because the mesh of the deformed chip is pre-defined in the simulation. For this same reason, the assumed geometry of the mesh may not be accurate, or a test may need to be performed to obtain the correct geometry, hence reducing the study to be semi-analytical in nature. Also, since the mesh is not updated, the simulation results cannot be employed in graphical animations of the actual chip separation and formation process. Moreover, results of the analysis are usually only available for the workpiece in the primary and secondary shear zone areas, and not in the newly formed surface or cutting tool.

The advent of computer-aided machining has created the need for a method to quickly obtain optimum cutting parameters for a variety of cutting conditions. For this purpose, FEM is a powerful tool. The current state of FEM technology in machining shows that most simulations rely on little or no empirical data. Although it has been successfully used in other metal forming operations, most metal cutting studies to date employ 2-D orthogonal cutting with continuous chip formation. Many studies have shown that simulated results are comparable to experimental results, but most of these results are limited to the range of cutting conditions applied. Thus, much research is still needed to generalize simulation results to a broader range of cutting conditions, with a comprehensive understanding of the

cutting process as the ultimate goal. Perhaps one day, FEM will be used to reliably predict cutting results for any combination of cutting conditions currently found in industry.

1.3 Research Approach

The objective of this research is to use the FEM technique to simulate the chip formation process in grooved tool metal cutting. The plastic flow behavior and the effect of groove geometry on the orthogonal cutting process will be analyzed. Particularly, attention will be paid to the chip flow characteristics and spatial distributions of stress and strain in the deformed chip. DYNA3D, a general purpose FEM code for three dimensional (3-D) nonlinear analysis of solid and structural mechanics, was used to generate the cutting model. With the help of symmetry planes, the elements in the model were restricted to two-dimensional (2-D) behavior.

This study is divided into two parts. First, an orthogonal cutting model with a flat-faced tool was generated. The simulated results were compared to published results in order to verify the validity of the model. These results will also served as a basis for comparison of simulations involving the grooved tool. The second part of this study investigated the effect of a grooved tool in the chip formation process. The effect of different groove geometries on the cutting process, such as groove depth and groove width, were also considered.

2 LITERATURE REVIEW

FEM was first introduced in 1973 in the field of machining when Klamecki [2] used it to model incipient chip formation in 3-D metal cutting. Since then, the FEM technique has been used to study incipient and steady state chip formation processes where most models were based on 2-D orthogonal cutting. The studies conducted so far dealt with various aspects of the FEM technique in cutting simulation, including the effects of varying cutting parameters, and the setup aspects of a FEM-based cutting model. Lajczok [3] developed a simplified model for orthogonal steady state cutting that used geometry and tool force measurements from experimental data. Because of its reliance on empirical data, this approach can be considered semi-analytical. The simulated results were limited to deformation behavior that did not account for material strain rate effects. Usui and Shirakashi [4] also developed a semi-analytical model for 2-D machining. They used the simulated results to predict 3-D behavior using the energy conservation approach.

Strenkowski and Carroll [5] modeled the first FEM simulation that analyzed the chip formation process from incipient to steady state cutting. The updated Lagrangian formulation was used to develop a 2-D orthogonal model. Since it did not rely on experimental data, it can be considered the first fully analytical FEM simulation in metal cutting. The problem was developed using the NIKE2D code [6] and the material model used was a thermoelastic-plastic material that included temperature effects. A parting line was incorporated where the chip was allowed to separate from the workpiece when a failure criterion based on effective plastic strain was satisfied. They also developed an Eulerian formulation with the same constitutive model for orthogonal cutting problem since excessive deformation caused convergence problems in the Lagrangian formulation [7]. The model was based on the work of Zienkiewicz [8, 9] in which the Eulerian formulation was used to study metal forming and extrusion problems. The workpiece material used was a viscoplastic material where elastic effects were negligible. Heat generated due to plastic deformation and friction at the tool-chip interface were also considered. Simulated results, limited to velocity vectors, effective strain rate and cutting force, were reported to compare favorably with experimental tests. This study did not enable the computer to animate the

chip formation process since the predetermined mesh was fixed.

A mixed Lagrangian-Eulerian formulation developed by Strenkowski and Moon [10] followed, making it the only work with a coupled Lagrangian-Eulerian formulation. They formulated a set of momentum equations that were applied to the flow field of both the Lagrangian and Eulerian description of the problem. This was achieved by defining relative velocities between the particle velocities in the FEM grid and the velocity or the grid itself. The work material used was an elasto-viscoplastic fluid, and the model did not use any empirical data, yielding results limited to steady state cutting without temperature effects. Nevertheless, the simulated results were in agreement with experimental data. Shih *et al.*[11] used the FEM method to study the chip formation process with strain-rate and temperature effects. The temperature effects were based on a linear finite element formulation where the thermal and material properties of the workpiece were assumed constant during cutting. The chip separation criterion was based on the distance between the tool tip and the nodal point connecting the two elements ahead of the cutting tool. For computational efficiency, they developed a rezoning technique that rearranged the mesh near the tool tip and the global mesh. Tool-chip interface friction effects were included in the model. Simulated results that showed concentrated high strain caused a shear band to initiate at the tip of the tool.

Komvopoulous and Erpenbeck [12] presented another orthogonal cutting model that employed a chip separation criterion based on essentially the same method employed by Shih *et al.*[11]. The study was based on quasi-static FEM simulations where emphasis was placed on analyzing the plastic flow, stress and strain distributions in the workpiece material. The published results presented a qualitative analysis of how these parameters were affected by a material model that included strain rate effects, friction at the tool-chip interface and a cratered tool due to wear. This study modeled the cutting tool with a built-up edge near the tool tip. Zhang and Bagchi [13] also developed yet another 2-D orthogonal cutting problem with chip separation based on the distance criteria, where chip separation is initiated when the distance between the tool edge and a leading node is equal or smaller than a critical value. From trial runs, the critical values were determined to fall between 10 to 30 percent of the elements length. The model also considered the tool-chip interaction in the sliding and sticking region at the interface. A constant coefficient of friction was employed to simulate sliding, and shear strength of the workpiece was used to simulate sticking. In a more recent paper [14], they proposed a separation criterion based on the ratio of the separation distance to the depth of cut.

Shih [15] presented a new technique for FEM simulation of metal cutting based on the "unbalanced force reduction method." This method required that external force vectors be applied to separate nodes

ahead of the tool tip where these forces function to keep the nodes together before separation. The magnitude of the force vectors was reduced incrementally as the tool tip approached these nodes, and the nodes would separate when the magnitude of the force became zero. Sliding friction was modeled with simple coulomb friction, while sticking friction was modeled based on the average maximum shear stress of the tool material, a similar method that was previously used by the author [11]. The study concluded that thermal stresses and cutting forces in the simulation influenced the prediction of residual stresses. Shih [16] also used the same modeling technique to study the effects of rake angle in orthogonal cutting. The published results showed that material-models with large strain, temperature, and strain-rate effects were not adequate to model cutting with a small rake angle. The proposed solution was to include fracture or damage effects to the work material. The author also pointed out that a simulation with a negative rake angle was not possible due the the large element deformation.

Many types of chip separation criteria have been used in FEM simulation of metal cutting processes, and they fall into two basic categories: geometrical criteria and physical criteria. Geometrical criteria are based on the distance between the tool tip and the immediate separating nodes. Physical criteria are based on physical variables such as stress, strain or strain energy. Huang and Black [17] investigated the effects of these criteria in machining simulation. Their results showed that the geometrical criteria caused early chip separation in incipient cutting, and the physical criteria resulted in late chip separation in steady state cutting. To solve that problem, the authors proposed an algorithm that combined the geometrical and physical criteria for a more accurate simulation.

3 METHODOLOGY OF SIMULATION

3.1 The Updated Lagrangian FEM Formulation

The updated Lagrangian formulation is in a fairly developed stage and is the choice of many FEM analysis programs for solid and structural mechanics. It has good numerical properties and is capable of effectively handling all kinematic nonlinear effects due to large deformation and large strains inherent to metal cutting analysis. However, it should be noted that whether a large strain behavior of the material is modeled appropriately depends on the constitutive law specified.

In linear analysis, the assumed displacement of the finite element mesh is infinitesimally small, and the material is linearly elastic. It is also assumed that the nature of the boundary condition does not change with the application of loads. Therefore, the finite element equation derived for the linear analysis is a statement of equilibrium for any specific point in time, and it is given by

$$\mathbf{KU} = \mathbf{R} \tag{3.1}$$

where $\mathbf{K}$ is the global stiffness matrix of the finite element assemblage, $\mathbf{U}$ is the nodal displacement vector of the system and $\mathbf{R}$ is the load vector of all the applied loads. The solution of this equation yields the nodal displacement vector $\mathbf{U}$, which enables the strains and stresses of the system to be calculated.

The global stiffness matrix $\mathbf{K}$ of the system is calculated from the direct addition of all its elemental components $\mathbf{K}^e$. Similarly, the global assemblage of load vector $\mathbf{R}$ is obtained by directly adding the elemental load vector $\mathbf{R}^e$. They can be expressed as

$$\mathbf{K} = \sum_i \mathbf{K}_i^e \tag{3.2}$$

$$\mathbf{R} = \sum_i \mathbf{R}_i^e \tag{3.3}$$

The elemental components are calculated with the following equations

$$\mathbf{K}^e = \int_V \mathbf{B}^{eT}\mathbf{C}^e\mathbf{B}^e dV \tag{3.4}$$

$$\mathbf{R}^e = \int_S \mathbf{H}^{eT}\mathbf{f}^e dS \tag{3.5}$$

where $\mathbf{B}^e$ is the strain-displacement matrix of element e, $\mathbf{C}^e$ is the elasticity matrix of element e, $\mathbf{H}^e$ is the the interpolation matrix of element e at the loaded boundary, and $\mathbf{f}^e$ represents all the elemental forces. These forces could include surface forces, body forces, thermal load, etc.. More details on this subject are available in the literature [18, 19].

The governing equation (3.1) represents the linear analysis of a structural problem where the displacement $\mathbf{U}$ is a linear function of the applied load $\mathbf{R}$. In nonlinear analysis such as in metal cutting, this linear relationship is no longer true since the assumptions of a small mesh displacement and of constant material properties are no longer valid. Thus, the system of equations needs to consider the changes in finite element assemblage, and also in the material property due to the nonlinear behavior of its strain and stress relation. In other words, matrix $\mathbf{B}^e$ and $\mathbf{C}^e$ in equation (3.1) are no longer constant. To handle the nonlinearity, the governing equation must be solved iteratively.

A general formulation that can be used for the solution process is the updated Lagrangian formulation which involves two general steps: (1) load increment, and (2) equilibrium iteration. The time variable is used as a reference to conveniently describe the loading and motion of the body.

The aim of the formulation is to obtain the solution of the equilibrium position at every time steps before updating to the next. The basic procedure is available in the literature [20], but summarized below.

If the solution at local increment n is known, the solution at load $\mathbf{X}_{n+1}$ can be obtained from the following linearized equation

$$[\mathbf{K}_t(\mathbf{X}^n)][\Delta u] = [\mathbf{R}(\mathbf{X}^n)]^{(n+1)} - [\mathbf{F}(\mathbf{X}^n)] \tag{3.6}$$

where

$[\mathbf{K}_t(\mathbf{X}^n)]$ = tangential stiffness based on geometry at t_n

$[\mathbf{R}(\mathbf{X}^n)]^{(n+1)}$ = external load vector based on the applied loading at t_{n+1} but geometry at t_n

$[\mathbf{F}(\mathbf{X}^n)]$ = stress divergence vector based on the displaced state and stress at load step t_n

$[\Delta u]$ = increment in displacement

$(\mathbf{X}^n)$ = coordinate vector at time t_n

Once $[\Delta u]$ is solved in equation 3.6, the coordinate vector is updated with the following equation

$$[\mathbf{X}^{n+1}]_0 = (\mathbf{X}^n) + s_0(\Delta u)_0 \tag{3.7}$$

where s_0 is a parameter between 0 to 1 obtained from a line search scheme. The new iteration for equilibrium now uses

$$[\mathbf{K}_t(\mathbf{X}_j^{n+1})]_j[\Delta u]_i = [\mathbf{R}(\mathbf{X}^{n+1})_i]^{(n+2)} - [\mathbf{F}(\mathbf{X}_i^{n+1})] \tag{3.8}$$

The subscript i indicates iterative number where j $\leqslant$ i. When the process converges, the coordinates are updated with

$$[\mathbf{X}^{n+1}]_{i+1} = (\mathbf{X}^{(n+1)})_i + s_i(\Delta u)_i \tag{3.9}$$

The load vector need not be a specified force vector. A boundary displacement or boundary velocity can be specified in which the equivalent load can be computed.

3.2 Chip Separation Criteria

Various chip separation criteria have been proposed in the study of FEM machining simulation and they can be grouped into two basic categories. One such category is a geometrical criteria based on the orientation of the element mesh. These criteria use the distance D between the tool tip and the nearest separating node, node a, on the predefined separation line as shown in Figure 3.1. If this distance is less than a critical value, then the node is allowed to separate. On the other hand, physical criteria are based on physical values such as stress and strain of the workpiece material in the element A ahead of the tool. Node a is allowed to separate when the value of the selected physical parameter exceeds the physical limit of the selected material.

The geometric criteria are very robust criteria and many researchers have used it in their models [4, 11–16]. However, their main disadvantage is their lack of physical laws governing the criteria. Thus, this has led other researchers to come up with the physical criteria. One such criteria proposed by Strenkowski and Carroll [5] were based on the effective plastic strain of the workpiece material. The authors reported that the failure criterion value in the range of 0.25 to 1.0 did not affect the final chip geometry but the larger strain value caused more residual stress to be imparted into the newly

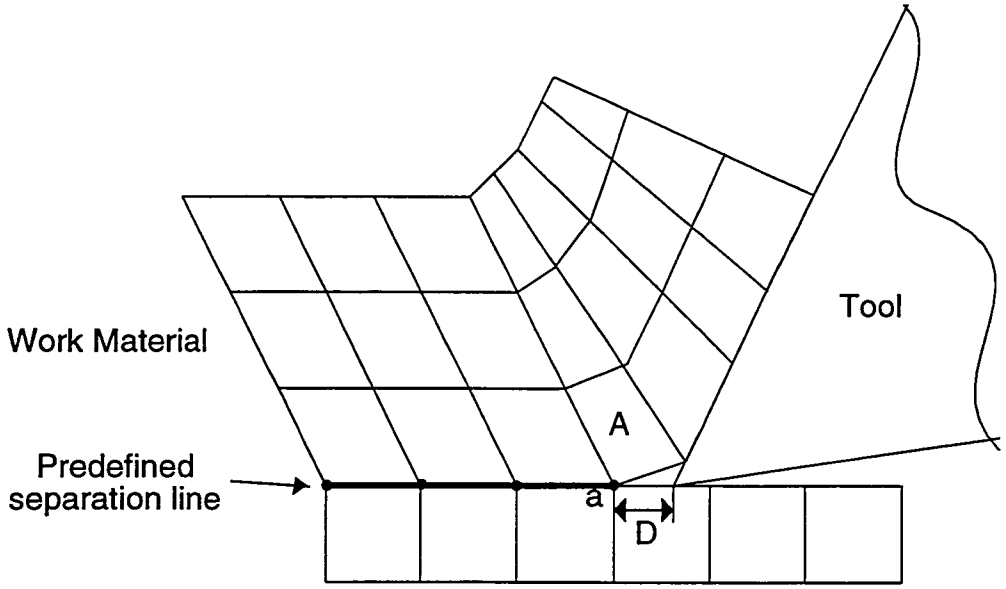

Figure 3.1 Chip separation criteria

generated surface. Another physical criterion based on energy was studied by Lin and Lin [21] where they established that the strain energy density is a material constant.

Huang and Black [17] conducted an extensive study on the chip separation criteria based on distance D (geometrical) or maximum shear stress ahead of the tool (physical). They concluded that if the magnitude of the distance criteria was too large, the chip would separate too early resulting in a crack in front of the tool tip. However, too small a magnitude would cause numerical problems due to severe distortion in the finite element mesh around the tool tip. For the criterion based on average maximum shear stress, nonconvergence would arise when the cutting tool penetrated into the workpiece at the beginning of cutting, causing a significant distortion of the mesh around the tool tip. However, the magnitude and the type of chip criteria used did not greatly influence the chip geometry and the stress and strain distributions in the workpiece. In contrast, determining the magnitude of the chosen criteria is important to simulate machining properly if the stress and strain magnitudes are to be determined correctly. Since either criteria do not greatly affect the simulation results in terms of the chip formation process, it is suggested that the geometrical criteria should be used in steady state cutting because its value is easier to determine (usually from trial and error). Nevertheless, Huang and Black [17] have proposed a combination of both the geometrical and physical criteria for incipient and steady-state cutting. The combination approach would avoid the early chip separation that results from the

geometrical criteria and late chip separation that results from the physical criteria.

3.3 Machining Simulation with the DYNA3D Code

DYNA3D is an nonlinear explicit finite element computer code for analyzing the transient dynamic response of three-dimensional solids and structures [22]. Unlike its implicit counterpart which forms and solves large matrix equations, it uses a large number of small time steps to obtain an explicit solution at each step thus requiring modest memory requirements. Because of this, there are no inherent limits to the size of model that could be analyzed, and problem size is only constrained by the available computer memory. This feature is extremely useful for metal cutting simulations because analyzing the chip formation process can require a large number of elements in the FEM model. DYNA3D utilizes three-dimensional(3D) finite element discretization of space and a finite difference discretization of time. The explicit central difference method, which is unconditionally stable, is used to integrate the equations of motion in time. The user is not required to specify the time step size at each solution step because this is internally handled by the code to minimize the number of time steps.

Boundary conditions in DYNA3D are specified by a "load curve". An arbitrary number of boundary conditions or loads may reference a single load curve and one load curve can contain any number of points. The boundary conditions can be specified for any of the following variables: force, velocity and displacement. This gives greater flexibility in modeling machining simulations by specifying the velocity of the cutting tool, the cutting force, or the displacement the cutting tool needs to traverse for a specified time. Generally, the velocity boundary condition is the most useful since this variable is easily controlled in actual machining. Another useful feature of the code is its use of constraints to prevent the translation or rotation of any part in a finite element assemblage. For instance, the cutting tool in Figure 1.1 can be constrained to move only in the x direction by preventing any translation in the y-axis to simulate the movement of the tool. Symmetry planes are also available to reduce the number of elements used in a model and thus the time of analysis. Loads due to thermal expansion can also be applied by specifying temperature changes in material models that include thermal expansion.

DYNA3D contains a robust and efficient capability to model general interface contact, a useful feature for machining studies. This capability enables one to simulate the separation of the chip from the workpiece and the sliding of the chip on the tool-chip interface. This contact problem is handled by "slide surfaces." Many slide surface options are available to treat the interactions between two surfaces, or between a surface and a set of discrete nodes. No limit is defined on the number and type of slide surfaces that can be used. Interface pressure distributions can be written to a DYNA3D post-processor

database and the forces of all nodes on the interface can be written to a file. This provides a convenient way to determine the forces over a segment or an entire area by defining a sliding surface in the section of interest.

A slide surface is created by defining a master surface and a slave surface or a set of slave nodes on the elements' faces where interface contact will take place. The distinction between the master and slave surface is that the slave surface (or nodes) is not allowed to penetrate the master surface. This is achieved through the use of two user-defined formulations: the penalty formulation or the Lagrangian formulation. When penetration is detected, the penalty formulation calculates a restoring force based on the depth of penetration, and the geometry and bulk modulus of the penetrated element. This force restores the penetrating node to the surface. The user is allowed to specify the amount of penetration allowed through a penalty factor. In the Lagrangian formulation, a restoring force is also computed, but it is determined by predicting the location of the penetrating node on the contact interface at the end of a time step, and then computing the contact force required to place the the node on the surface at the end of the time step.

Two types of slide surfaces that are especially useful for the simulation of machining are the *sliding with separation and friction* slide surface (type 3) and the *tied with failure* slide surface (type 9). The type 3 slide surface is based on the penalty formulation, and two bodies, either initially separated or in contact, are allowed to join or separate in any arbitrary fashion. Large relative motions are permitted and coulomb friction, μ, can be specified based on

$$\mu = \mu_k + (\mu_s - \mu_k)e^{-\beta v_{rel}} \tag{3.10}$$

where μ_s and μ_k represent the static and kinetic coefficient of friction, β a coefficient governing the rate of change from static friction to kinetic friction, and v_{rel} is the relative velocity of the sliding surfaces. This option is useful in modeling the interface contact friction between the chip and the tool face.

The type 9 slide surface is useful to simulate chip separation. It is an option also based on the penalty method formulation that ties two surfaces together until a failure criterion is satisfied. This criterion is given by

$$\left(\frac{F_n}{F_{nf}}\right)^2 + \left(\frac{F_s}{F_{sf}}\right)^2 \geqslant 1 \tag{3.11}$$

where F_n and F_s are the total normal and shear forces acting on the segment, and F_{nf} and F_{ns} are the normal and shear failure forces of the segment. These values are computed internally based on the

segment area, and the material ultimate tensile and shear strength provided by the user. When the criterion is met, the slide surface will break and then function as a type 3 slide surface.

Obviously, the choice of a material model is important in a FEM machining simulation. An elastic-plastic model is used most often where the workpiece material is assumed to have an elastic range characterized by a modulus of elasticity and a clearly defined yield point after which the region is characterized by strain hardening and strain softening due to plastic deformation. DYNA3D offers a number of material model options such as a kinematic/isotropic elastic-plastic model that includes linear strain hardening due to kinematic and isotropic hardening. Other useful option is the elastic-plastic model with thermal effects where material properties are dependent on temperature. Additional details can be found in the literature [22].

3.4 Finite Element Model

A FEM simulation of chip formation with a flat-faced cutting tool was carried out using DYNA3D. Although this software is designed to model 3-D simulations, it was restricted to analyze a 2-D orthogonal cutting problem in this study. With a few modifications, however, the model can be extended to 3-D for future research. The workpiece was modeled with an isotropic elastic-plastic material with the properties of 2024-T4 aluminum alloy. The cutting tool was modeled as a sharp tool with elastic material properties. It was assumed that the tool was much stiffer than the workpiece material, as is generally the case in metal cutting practices. Therefore, the tool's modulus of elasticity was set at a much larger value than that of the workpiece. Both workpiece and tool were modeled with eight-node "brick" solid element in the initial setup as shown in Figure 3.2. A total of 562 elements were used of which 12 of them belonged to the tool.

The depth of cut was set at 0.25 mm and rake angle for the cutting tool was set at 20 degrees. To simulate cutting, the tool was assumed to move in the negative x direction and the workpiece was assumed to be stationary. Tool motion was modeled by prescribing a velocity of 260 mm/s with a single "load curve". Constraints were placed on the tool so that no movement was allowed in the y or z directions. Constraints were also placed on the left face and bottom face of the workpiece so that no movement was allowed in any direction. A clearance was also provided at the tool flank with a clearance angle of 5 degrees.

During the cutting process, the tool penetrates into the workpiece. When the chip (segment A) separates from the workpiece, it comes in contact with the tool-chip interface c-d. For the chip to slide along this interface without penetrating into the tool material, a contact surface must be defined,

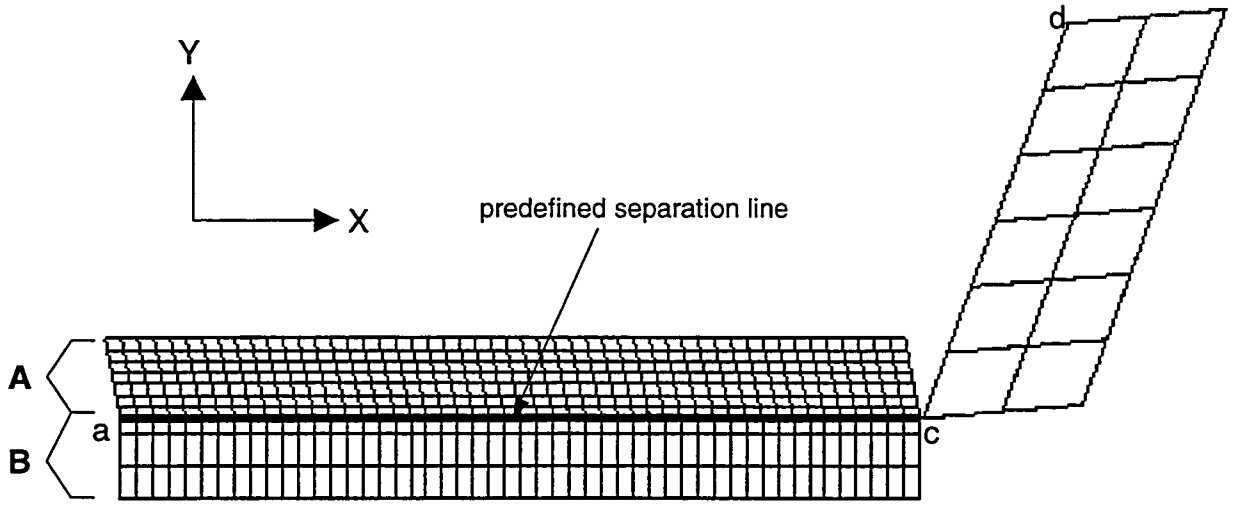

Figure 3.2 Setup of flat-faced tool cutting simulation

so the type 3 slide surface was used. Tool face c-d was defined as the master surface and the lower face of segment A on line a-c was defined as the slave surface. Between the two slide surfaces, a simple static friction coefficient based on Coulomb friction law was employed. This was achieved with the built-in frictional condition shown in equation 3.10. By specifying μ_k and β to be zero, a rate-independent friction model is obtained with $\mu = \mu_s$. If the value of this coefficient was too large, excessive friction would result in numerical instability due to large distortion in the grid. Several trial runs were performed and a friction coefficient of 0.1 was chosen for the final simulation. This relatively low value is representative of a well lubricated surface where there is little or no adhesion between the tool and chip. Temperature effects in this study were ignored.

In order to simulate chip formation, segment A must be allowed to separate from segment B in the workpiece when a separation criterion is met. This is achieved by prescribing a slide surface on the predefined chip separation line a-c. A type 9 slide surface option was used for this purpose. The lower face of segment A on line a-c was defined as the slave surface. The upper face of segment B on the same line was defined as the master surface. Since the objective of this study was to simulate the chip formation process from incipient to steady state cutting, the chip separation criterion was adapted from the algorithm suggested by Huang and Black [17], namely a combination of the geometrical and physical criteria. The algorithm for combining the two criteria is illustrated in Figure 3.3. The physical criterion is based on equation 3.11 which is provided with the type 9 slide surface. The ultimate tensile

strength and ultimate shear strength of the workpiece material, 303 MPa and 150 Mpa, respectively, were used in equation 3.11 to define the physical criterion for separation of surfaces.

The geometrical criterion is satisfied when the distance between the tool tip and the immediate separating node ahead (distance D in Figure 3.1) is less than a critical value. However, no physical basis is available to determine the exact value. In most machining studies conducted where the geometrical criteria was used, the critical distance was found through trial and error. Zhang and Bagchi [14] suggested that the value should be approximately 10 to 30 percent of the workpiece elemental length. In this study, the value of this distance was obtained from several trial runs with the value set between zero to 30 percent of the workpiece elemental length. It was observed that at less than 10 percent, the finite element mesh suffered large distortion. When the value was set between 10 to 30 percent, the numerical stability improved and the analysis time also decreased. However, when the value increased from 10 to 30 percent, the size of the crack ahead of the tool tip also increased. In actual cutting of ductile material, this crack is not formed in steady state cutting. Thus, the critical value of this study was chosen at 10 percent of the elemental length so that the crack is minimized but not at the expense of severe elemental distortion.

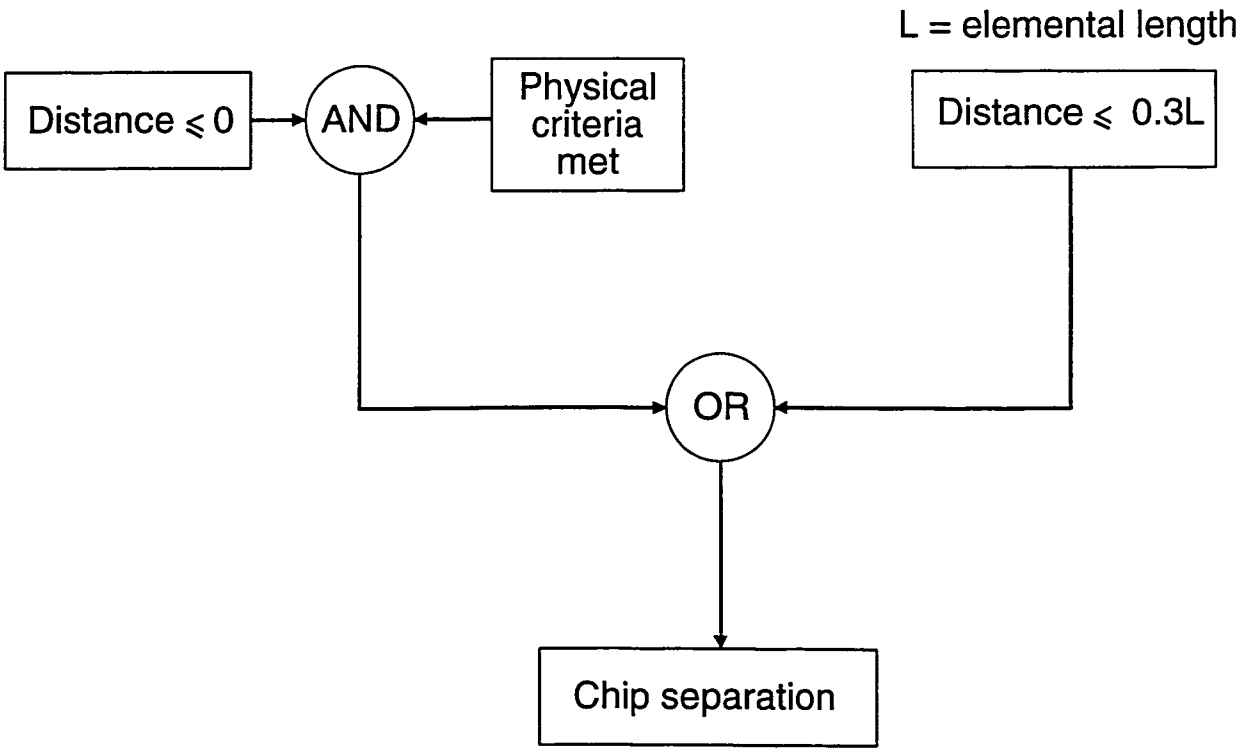

Figure 3.3 Algorithm for chip separation

4 FLAT-FACED TOOL SIMULATION

The results of a flat-faced tool simulation are presented first to serve as a basis for comparison with later simulations of grooved tool cutting. Figures 4.1(a), 4.1(b) and 4.1(c) show a time history of the simulation process where the progression of the chip formation is seen from the incipient cutting stage to the final stage where steady-state cutting has been reached. Examination of the elemental shape and of the general shape of the chip in these figures shows the development of a primary deformation shear zone extending from the tool tip to the free surface of the chip, and also curl development in the chip. These deformed meshes allow the qualitative assessment of the physical behavior in the chip formation process at every time step, where chip curling and localized shear flow can be observed. The tool required 6480 time steps to travel a distance of approximately 1.5 mm as shown in Figure 4.1(c). Although the mesh in Figure 4.1(c) shows large deflection in the deformed chip, it is not exaggerated since the magnification factor is equal to one. Despite the large deflection, the element deformation in the chip is not excessive. The front elements of the chip experienced the most distortion. Transformation from rectangular to triangular shape in the elements indicates the presence of intense compression in the initial stage of cutting. However, this observation is not isolated to this study as results from other published studies have also displayed similar behavior. When steady state cutting was achieved in Figure 4.1(b), the mesh distortion became uniform. Most of the near-rectangular elements were transformed into parallelograms when passing through the primary shear zone, which indicates that the elements experienced shear and compression. Similar deformation patterns have been observed in FEM machining studies using the Lagrangian formulation, and also in Lee's experiments using chips with imprinted gridlines [23].

The isostrain contours of effective plastic strain in the deformed mesh corresponding to Figure 4.1 are shown in Figure 4.2. From the progression and orientation of the strain contours, the amount of plastic work from incipient cutting to steady state cutting can be observed. From the spatial distribution of the contours and strain distribution shown in Figure 4.2(c), two distinct deformation zones are also observed. The first is the primary deformation zone that extends from the tool tip to the chip free surface. The strain magnitude of the elements in this zone increases as they pass through the primary

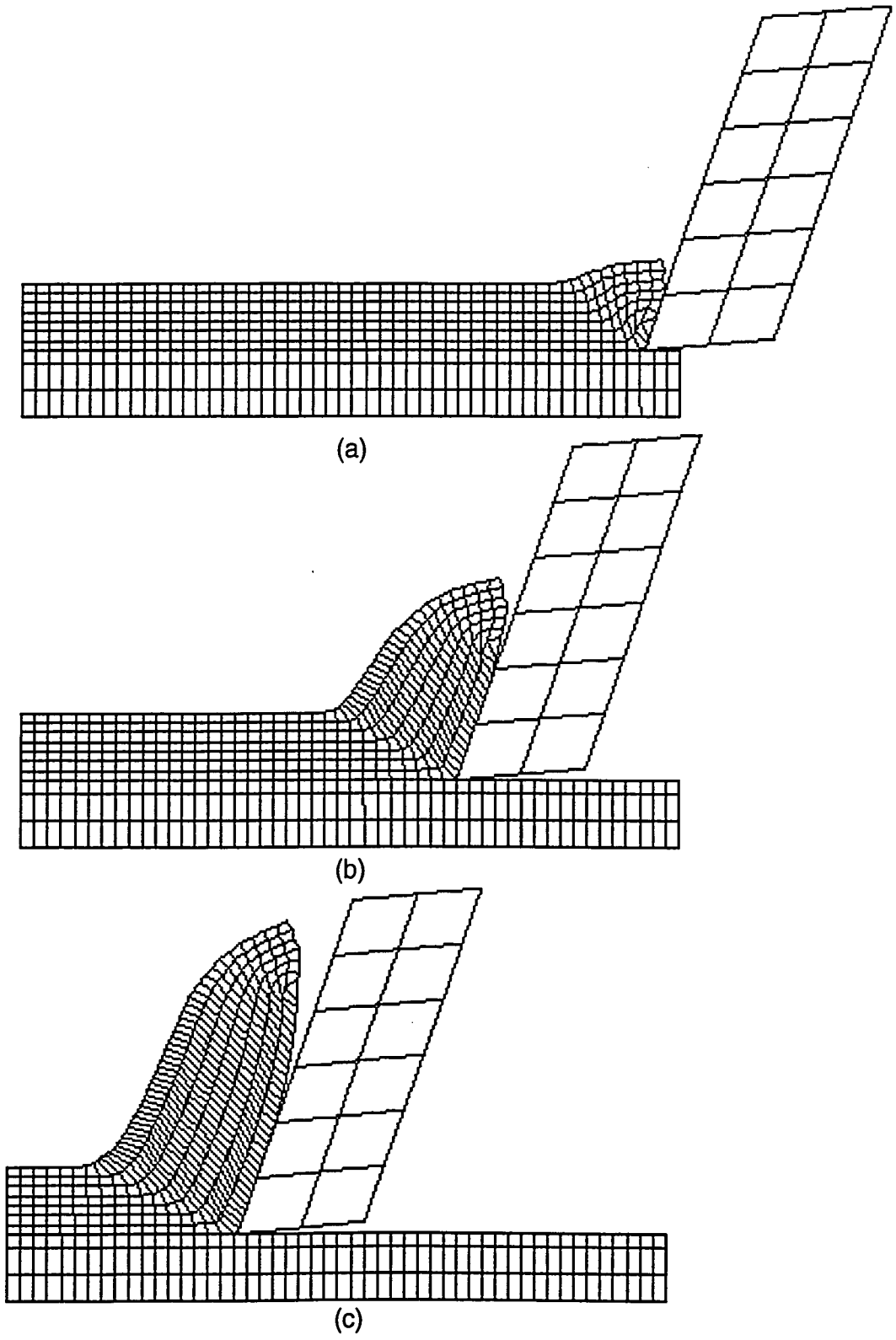

Figure 4.1 Chip geometry of flat-faced cutting simulation

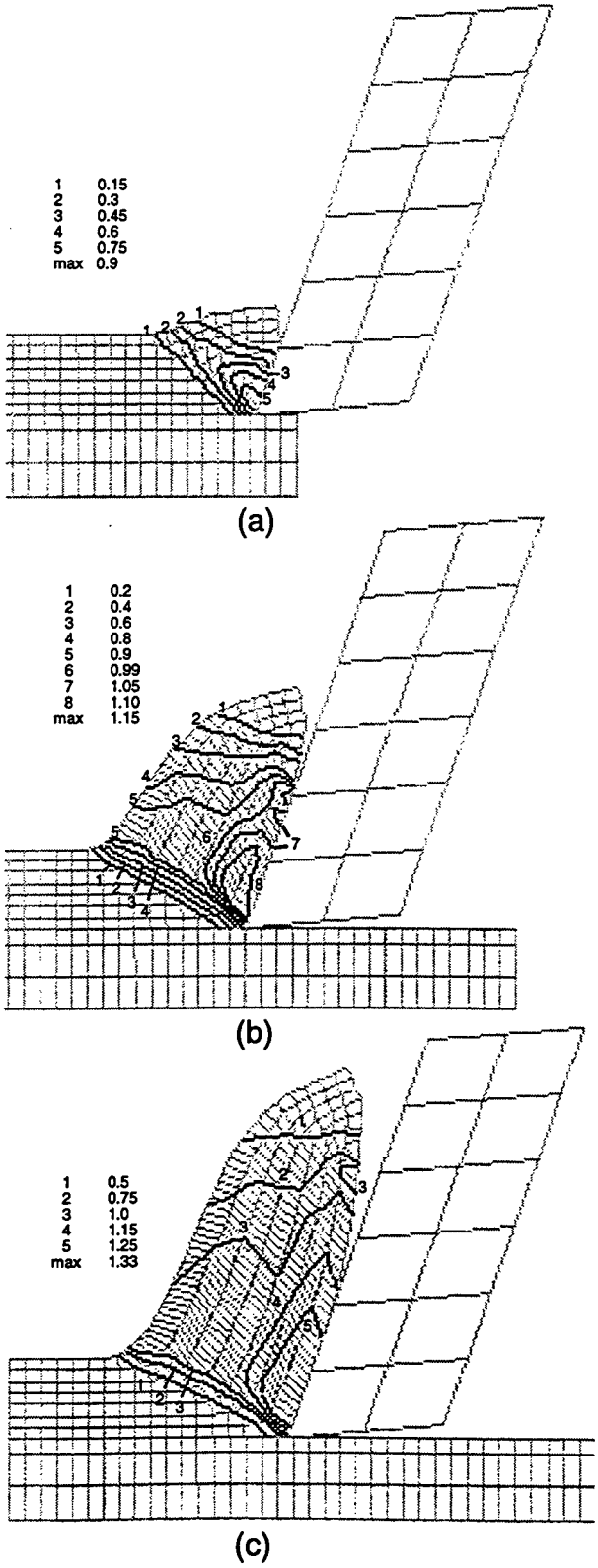

Figure 4.2 Effective plastic strain contours

shear zone to a magnitude of approximately 0.9 to 1.0. A secondary shear zone with maximum strain magnitude of 1.33 also developed in the vicinity of the tool-chip interface. This is consistent with the elemental shapes in this vicinity that displayed the most distortion. After the elements in this region went through the primary shear zone, they were further distorted by a compressive force caused by the tool movement into the workpiece. This force created a bending moment that further sheared them in the vertical direction as shown in Figure 4.3. The fact that the secondary shear zone occurred at the bottom of the chip indicates that the frictional force at the interface inhibited the upward flow of the chip, thus imparting more plastic deformation in the elements contacting the interface. Nevertheless, the distortion of elements was not excessive enough to cause sticking between the chip and tool. This is consistent with the earlier modeling assumption where the defined friction coefficient of 0.1 indicated a well lubricated condition that was not sufficient to induce an adhesion force.

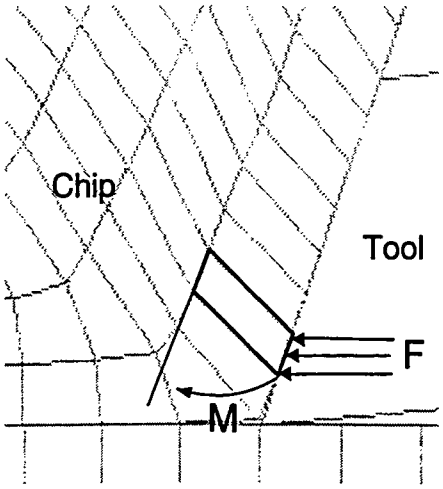

Figure 4.3 Enlarged region near tool tip. Compressive force F from tool creates bending moment M

The isostress contours of effective stress and maximum shear stress corresponding to Figure 4.1 are shown in Figures 4.4 and 4.5. Comparing the spatial variation and distribution of the contours in both figures, the contours exhibited similar patterns. The only major difference observed was in their magnitudes. Higher stress magnitudes were found in the vicinity of the primary and secondary deformation shear zone. The primary shear zone had a maximum shear stress value of approximately 450 Mpa, or 50% greater than the material strength of 300 Mpa. This is not unexpected because the greater stress is caused by the strain-hardening effects that are included in the material model.

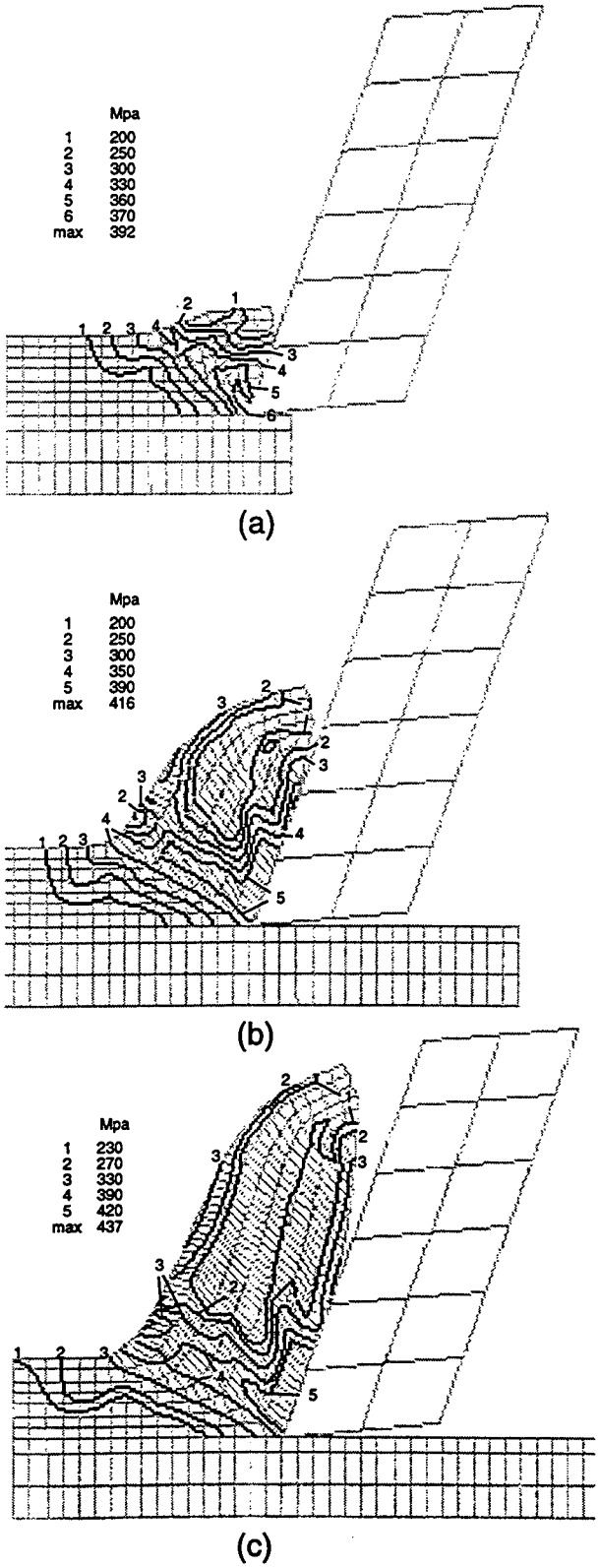

Figure 4.4 Effective stress contours

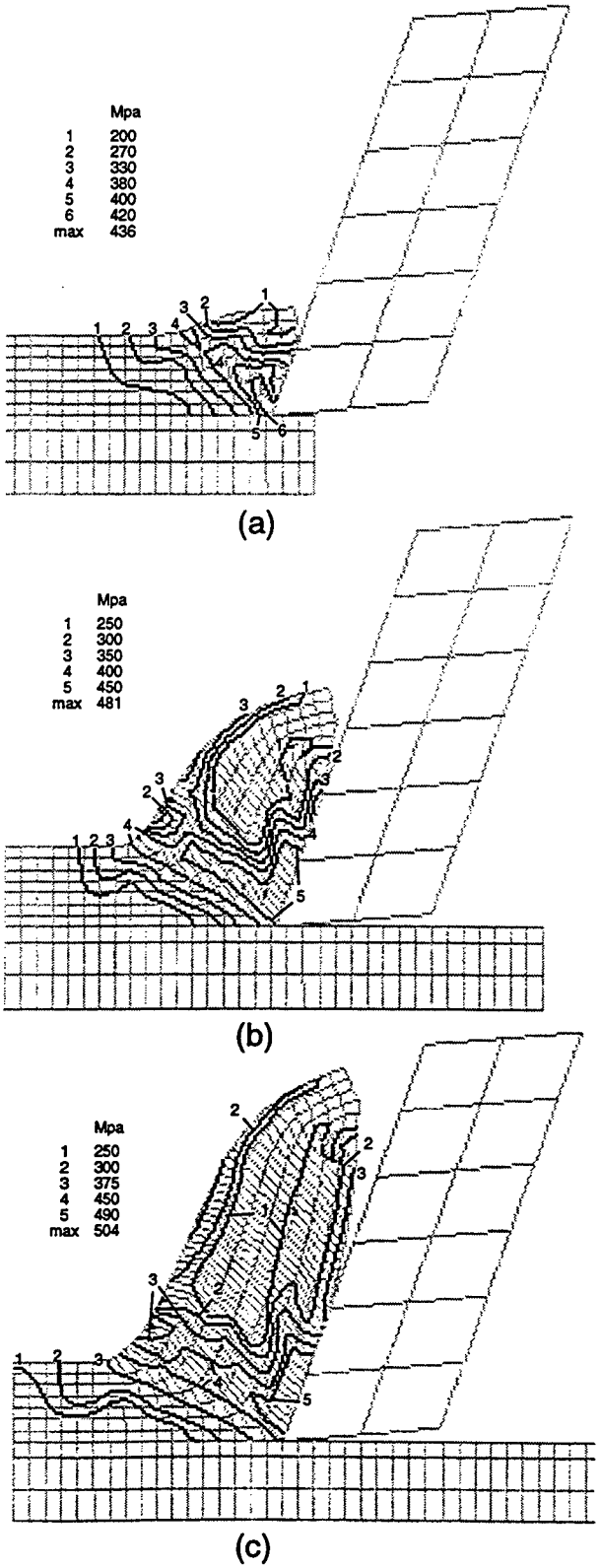

Figure 4.5 Maximum shear stress contours

The maximum shear stress region of approximately 490 Mpa was located near the tool tip, and it was not confined to an excessive shear plane as predicted by metal cutting theory. Residual stresses were also present in the chip after it leaves the tool-chip contact surface, which is in agreement with actual machining. However, no residual stresses were detected in the newly machined surface. The reason for this lack of residual stresses is that the separating node closest to the tool tip was able to separate early enough so that minimal tool forces were transmitted to the subsurface of the machined workpiece to cause permanent deformation. Nevertheless, since the primary focus is on the characteristics of the chip to ultimately predict chip breakability, the effect of residual stresses in the new surface is negligible.

Note that the flat-faced tool simulation also predicts the shape and thickness of the deformed chip. Significant chip curl is observed and the deformed chip thickness is greater than undeformed thickness. It is instructive to see how much of the effective or shear stress were caused by tensile or compressive stress components. Normal stress contours in the XY plane of the simulation are shown in Figure 4.6. The difference between the maximum tensile and maximum compressive stress was of less than 1%. Comparing the stress distribution with that of Figure 4.5(c), the compressive component was dominant in the primary shear zone and the tensile component was dominant in the secondary shear zone.

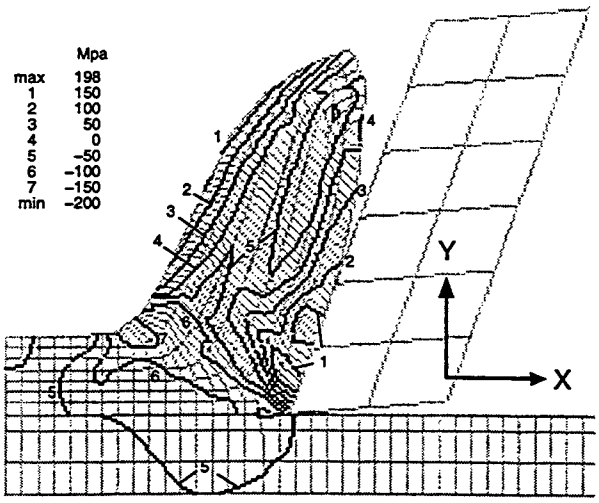

Figure 4.6 Normal stress contours in the XY plane

5 GROOVED TOOL SIMULATION

Chip control is an important issue in machining operations because of the need to predict chip breakability. This is particularly true in the machining of ductile materials since such operation tends to create long chips that could become entangled in the machine, thus, potentially causing delays in the assembly line and also compromising the safety of the operator. In applications where a good surface finish is important, stray chips can scratch the part. Also, the scratch sites are notorious for causing stress concentration in machine parts which can lead them to fail prematurely. Therefore, chip control entails breaking of chips to prevent the formation of long, continuous chips, and removing the chips to prevent damage to the machined parts.

A continuous chip will not break if it is permitted to curl naturally. Thus, the basic approach to inducing chip fracture is to direct the chip towards an obstacle to produce a bending stress for breaking. Many means are available to do this, such as changing the cutting parameters to direct chip flow into an obstacle, usually the workpiece surface or tool holder. One popular method of chip breaking is to clamp an obstruction-type chip breaker on the the tool as shown in Figure 5.1(a). The chip breaker serves two purposes: (1) it imparts a bending force on the chip to promote breaking, and (2) it directs the chip into the workpiece surface to break it against the surface. The advantage of using this type of chip breaker is that it can be adjusted for a wide range of feed rates. However, much time and effort is required for setup or readjustment. The more commonly used chip breaker today is a grooved cutting tool in the form of tool insert as shown in Figure 5.1(b). By reducing the curvature of the chip, the grooved tool is able to direct the chip more effectively towards an obstacle. The groove also produces a thicker chip section which promotes breaking. The advantage of a grooved tool chip breaker is that it requires no setup, increases the effective rake angle and reduces the tool-chip contact length [24]. This in turn reduces the required cutting forces and increases tool life when compared to flat-face, negative rake tool inserts.

Figure 5.2 shows the geometry that characterizes a grooved tool. The land width is the most critical parameter because it determines the feed rate and, thus, the amount of material removed in a single cut.

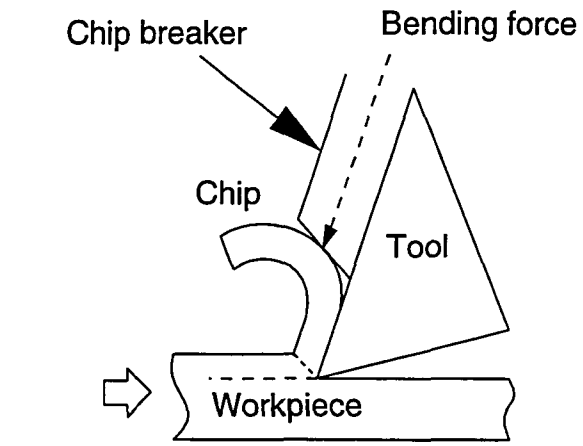

(a) obstruction chip breaker

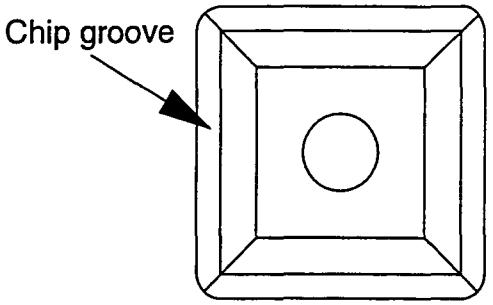

(b) grooved tool insert

Figure 5.1 Types of chipbreaker

Larger land widths are used for roughing cut since they increase the strength of the tool. Smaller land widths are used for finishing cut to ensure that chips flow into the groove. The less critical parameters are the depth and backwall height. Generally, their values should be increased in rough cutting to impart a greater bending stress in the chip.

A FEM study of the chip formation process in grooved tool orthogonal cutting was performed in three different simulations. Each simulation considered the effects that different groove parameters had on the stress and strain distributions in the chip formed. The first simulation was modeled to simulate grooved tool cutting and compared the results to flat-faced tool cutting. This simulation also served as a basis for comparison for the second and third simulations, where the groove depth and width were changed. Overall, the intent of the three simulations combined was to analyze the basic aspects of

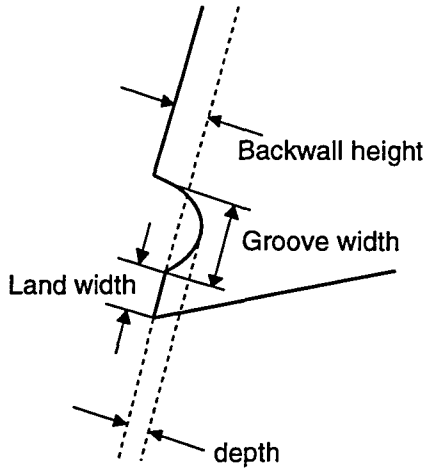

Figure 5.2 Parameters of a grooved tool

grooved tool cutting. The analysis results are presented in terms of the evaluation and comparison of the chip flow characteristics (chip curl, shape, thickness, etc.), stress and strain distributions.

5.1 Effect of Grooved Tool in the Chip Formation Process

In the first simulation, a groove was modeled into the flat-faced cutting tool used in the previous simulation as shown in Figure 5.3. The elements in the tool were increased from 12 to 20 so that a sufficiently smooth groove could be generated. The groove was modeled with a width of 1 mm, a depth of 0.14 mm, and a rake angle of 0 degree. Land width was not considered in the simulation. When land width is included, a sharp corner on the leading edge of the groove causes the slope to change abruptly, which in turn causes the chip elements to undergo excessive deformation when sliding into the groove, thus yielding numerical problems. The workpiece elements were tilted slightly to the right in anticipation of the excessive chip deformation when the elements passed through the primary shear zone. Such "counter distortion" elements were also used in several other studies [5, 10, 11–12, 15–16]. The degree of tilt was determined from several trial runs until no excessive deformation was observed in the deformed chip. All other parameters from previous flat-faced simulation such as cutting speed, depth of cut, chip separation criteria and tool-chip interface friction coefficient were kept constant in this model.

The final tool position of the first simulation is presented in Figure 5.4. Figure 5.4(a) shows the

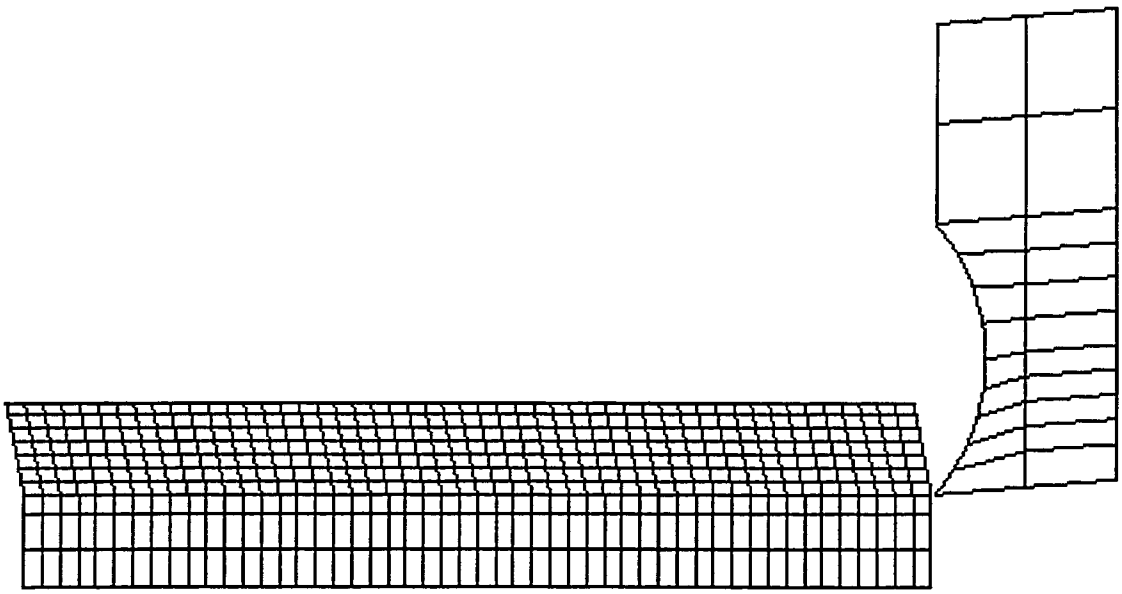

Figure 5.3 Initial setup of grooved tool cutting

mesh geometry and 5.4(b) shows the isostrain contours of the effective plastic strain in the workpiece. Although the rake angle at the lower edge of the groove was comparable to the rake angle in flat-faced tool cutting simulation, the rake angle became smaller and in fact turned negative when it approached the upper edge of the groove. This reduced the effective rake angle for cutting and thus increased the deformed chip thickness as observed in Figure 5.4(a). The increase in chip thickness was also caused by greater frictional effect due to longer tool-chip contact length. The increase in contact length is noticeable when comparing Figures 5.4(a) and 4.1(c). Consequently, thicker chip sections reduced the shear angle in the primary deformation zone. The shape of the chip also conformed closely with the groove geometry even though a slight gap existed at the upper edge of the groove. As expected, the groove imparted more curl into the chip when the chip flowed into the groove where it was later deflected at the upper edge to form the curl.

The maximum effective plastic strain region was concentrated on the free surface, the point where the chip started to flow upward and bent as shown in Figure 5.4(b). The maximum strain value is approximately 1.42 as compared to 1.33 in Figure 4.2(c). The secondary shear zone is no longer evident in the figure. The reason why a maximum strain did not exist near the interface is because the compressive force the tool exerted on the chip now served to bend it, and not so much to shear it. Since the chip can be modeled as a curved beam, a tensile force was created at the lower chip surface

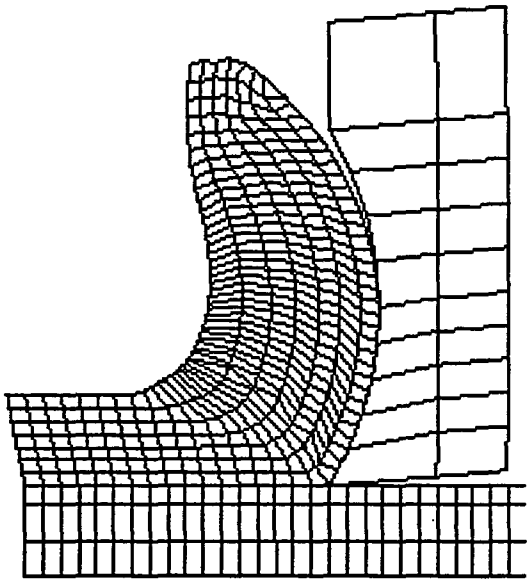

(a)

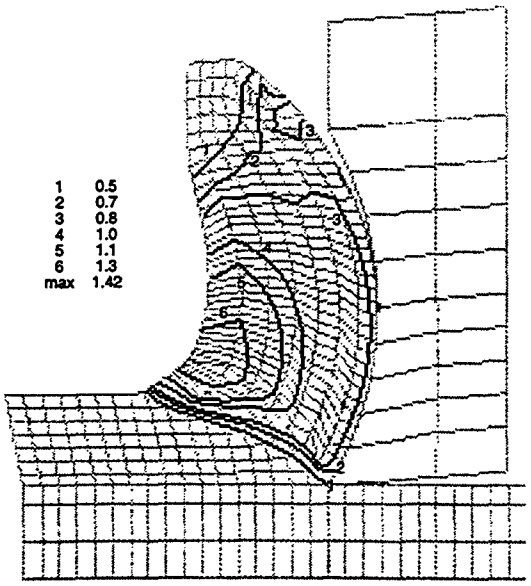

(b)

Figure 5.4 First simulation: (a) mesh geometry at final tool position. (b) effective plastic strain contours.

due to bending. The tensile force tends to stretch the chip near the lower surface and compress the elements near the upper surface. This is evident from the elemental shapes in both region. The shape of the elements near the interface appeared more rectangular, in contrast to the parallelepiped shape displayed in Figure 4.2(c). On the other hand, the element shape in the free surface region is longer, indicating that there was severe compression in the region.

Figures 5.5(a) and 5.5(b) show the isostress contours of the maximum shear stress and normal stress corresponding to the mesh geometry in Figure 5.4(a). In Figure 5.5(a), the maximum shear stress coincided with the region of maximum strain in Figure 5.4(b). The magnitude of the maximum shear stress was 498 Mpa, approximately 25% more than the shear stress magnitude of 350 Mpa to 400 Mpa near the tool tip and interface region. Examining Figure 5.5(b), the shear stress in the maximum strain region was greatly influenced by compressive stress, whereas the region near the tool tip was mostly affected by tensile stress. However, the compressive component is about 70% greater than the tensile component, unlike the flat-faced tool simulation where both components were almost equal.

5.2 Effect of Increased Groove Depth

In the second simulation, a deeper groove was used to investigate the effect of groove depth on the chip formation process. The depth was increased from 0.14 mm to 0.2 mm while all other parameters used in the first simulation remained constant. Thus, the results in this simulation (chip flow characteristics, strain and stress distributions) are contrasted to the results in the first simulation. Figures 5.6(a) and 5.6(b) show the chip geometry and isostrain contours of the effective plastic strain, respectively. Comparing Figure 5.6(a) to Figure 5.4(a), the shear angle of the primary shear zone has decreased. The deformed chip section is also thinner and more uniform throughout. Although the deformed chip thickness appears similar to the undeformed thickness, careful examination shows that the deformed section is thicker. Also, the chip curl has increased, which is not surprising since the chip's shape conformed closely to the smaller radius of curvature due to a greater groove depth.

When comparing the strain distribution and the strain magnitude in Figures 5.6(b) to 5.4(b), the location of the maximum effective plastic strain still exists in the upper surface of the chip. However, the maximum strain value has decreased to 1.09. The strain value at the interface has also decreased to 0.5, approximately 37% of the interface strain value in the first simulation. The lower value of strain distributions is consistent with the less severe elemental deformation observed in Figure 5.6(a). While the magnitude of the strain may be different, the strain distribution were quite similar. The isostress contours of the maximum shear stress and normal stress are shown in Figures 5.7(a) and

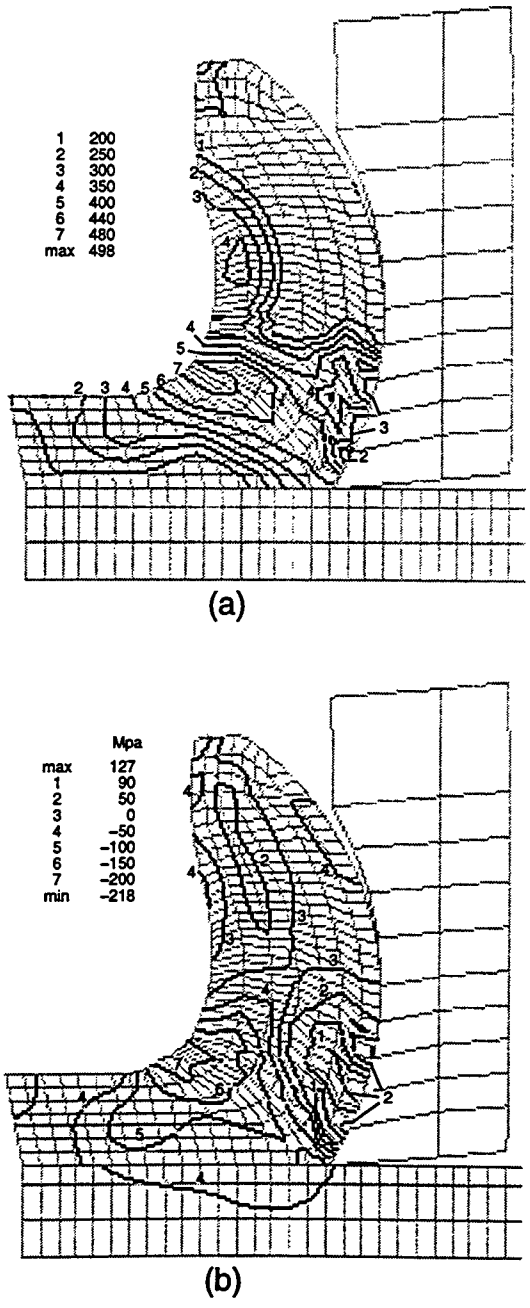

Figure 5.5 (a) maximum shear stress contours. (b) normal stress contours.

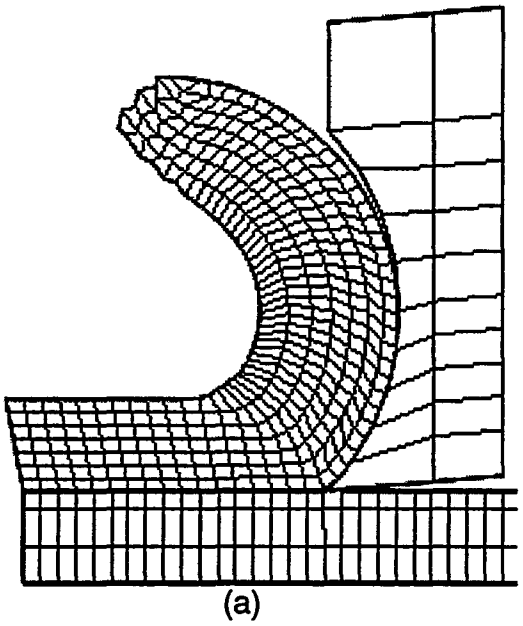

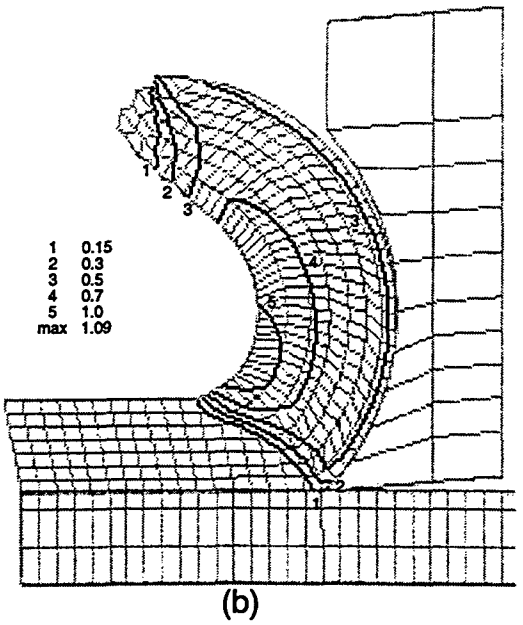

Figure 5.6 Second simulation: (a) mesh geometry at final tool position. (b) effective plastic strain contours.

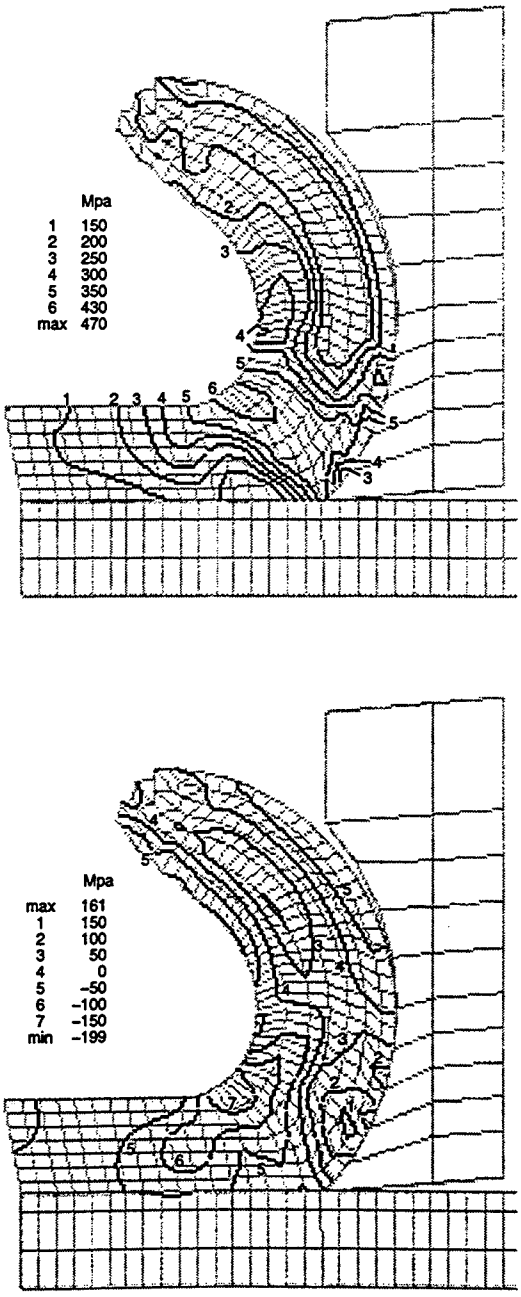

Figure 5.7 (a) maximum shear stress contours. (b) normal stress contours.

5.7(b). Comparison between Figures 5.7(a) and 5.5(a) shows that the maximum shear stress value in the maximum plastic strain region is also reduced. A higher shear stress region is not evident near the tool tip indicating that a secondary shear zone did not exist. Comparing Figures 5.7(b) and 5.5(b), the region of compressive stresses remained near the upper chip surface and the tensile normal stresses remained near the tool tip. However, the maximum tensile stress has increased and the maximum compressive stress has decreased relative to the previous simulation. This implies that an overall tensile stress was added during the chip formation process. Nevertheless, the increase in tensile stress indicates that the deeper grooved tool exerted a greater bending force on the chip.

5.3 Effect of Reduced Groove Width

The third simulation was modeled with the same cutting parameters used in the first simulation, except for the groove width that was reduced from 1 mm to 0.75 mm. The mesh geometry and effective plastic strain contours corresponding to the final tool position are shown in Figures 5.8(a) and 5.8(b). In order to investigate the effects of a smaller groove width on the chip formation process, these figures are contrasted to Figures 5.4(a) and 5.4(b). Comparing Figure 5.8(a) to 5.4(a), the deformed chip still conforms closely to the groove geometry but the gap that existed near the upper edge of the groove has disappeared. Therefore, it can be concluded that the chip was formed under the full influence of the groove. A good estimate of the shear angle is not easy since the strain contours in the primary shear zone area are ill defined. Chip thickness and curling have also increased. Examination of the chip free surface where curling started revealed that the elemental shapes were much longer and thinner. Such elemental transformation indicates the presence of an intense compressive force in the region. Since element distortion is most noticeable in this region, this also implies that the elements have undergone severe plastic deformation, and the plastic strain value would be at a maximum. This is confirmed by the strain distribution shown in Figure 5.8(b). Although the strain distribution contours are similar to those in Figure 5.4(a), the maximum strain magnitude in the chip's free surface has increased. However, the strain value near the interface has decreased by more than 50%. Recalling that the chip can be modeled as a curved beam, a greater chip curl would cause more surface tension to be induced in the lower chip surface. This tensile stress would offset the shearing stress due to the interface friction experienced by the elements, thus inhibiting plastic deformation.

The maximum shear stress contours corresponding to Figure 5.8(a) are shown in Figure 5.9(a). Similar to all previous simulations, the largest maximum shear stress is located in the region of maximum strain and apparently, the maximum shear stress also increased because of greater element deformation.

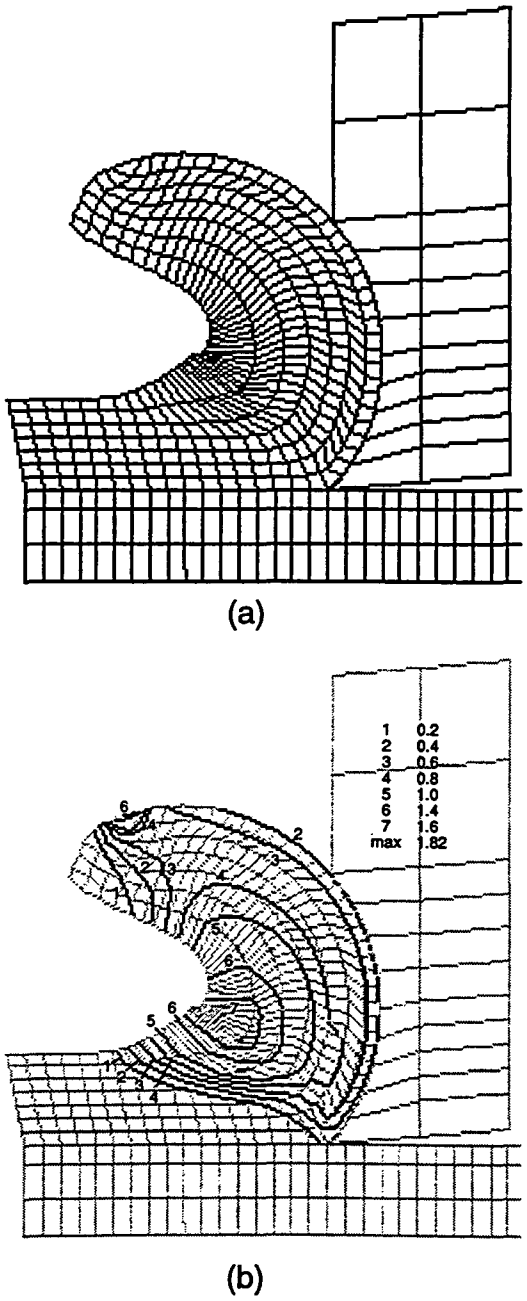

Figure 5.8 Third simulation: (a) mesh geometry at final tool position. (b) effective plastic strain contours.

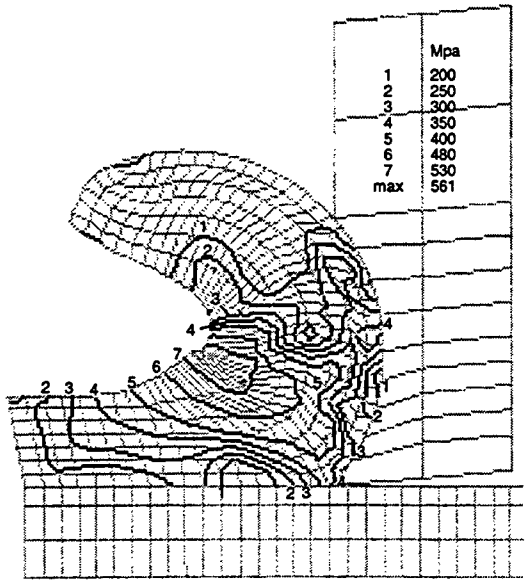

(a)

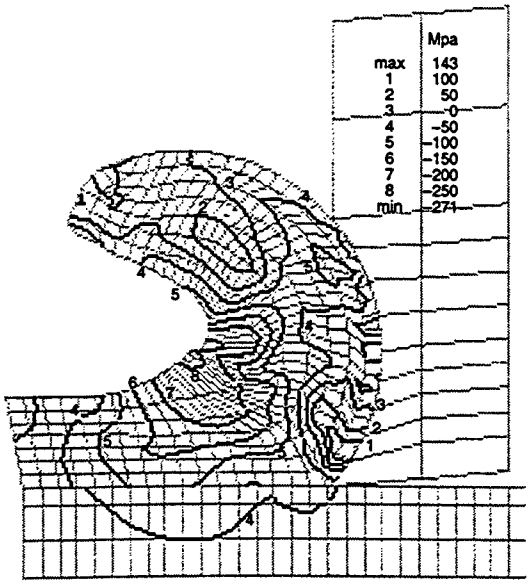

(b)

Figure 5.9 (a) maximum shear stress contours. (b) normal stress contours.

The corresponding normal stress contours in Figure 5.9(b) showed that this region is still in the influence of compressive stress, which also confirms the result of thin and long elemental deformation mentioned earlier. Comparing Figure 5.9(b) and 5.9(a), the tensile stress region still exists near the tool tip. Although the overall magnitude of the compressive and tensile normal stresses increases, the ratio of largest compressive to largest tensile stress has changed. This also indicates that the rate of change in both components is not linear. Given a smaller groove width and the same groove depth, the groove radius of curvature is reduced. Thus, the groove imparts more curl on the chip. However, a smaller groove also restricts the upward chip flow, thus increasing the chip thickness. The combined effect of a curlier and thicker chip section increased more of the compressive stresses.

6 CONCLUSION

Four FEM simulations of machining were presented in this study. They demonstrate that FEM is a useful approach to study the chip formation process in grooved tool cutting. The following conclusions can be drawn from the analysis.

1. The first simulation involved the development of a finite element model for a flat-faced tool simulation in orthogonal cutting. The model accounted for chip separation, material behavior of elastic-plastic with isotropic strain hardening, and sliding interface frictional condition. Cutting was simulated with the Lagrangian approach, where the tool was displaced incrementally from incipient to steady-state cutting. The chip separation criteria used a combination of geometrical and physical criteria, which was adapted from the algorithm suggested by Black and Huang [17]. Analysis results were presented and discussed in terms of effective plastic strain, maximum shear stress and normal stress distribution.

2. The 3-D code DYNA3D was employed to generate 2-D results comparable to other published work. The developed finite element model can, in fact, be easily extended to investigate 3-D machining such as oblique cutting.

3. The remaining simulations investigated the effects of a grooved tool on the chip formation process. These simulations used the same modeling technique from the first simulation. Apparent chip curling was observed with grooved tool cutting. The grooved tool imparted a greater bending force on the chip which increased the compressive and tensile stresses at the chip root. This is in fair agreement with experimental results that show most chip breaking occurring at the chip root [25]. Although compressive stress is more prominent, it is not clear whether the chip would break under the influence of tensile or compressive stresses, thus suggesting an area for future research.

4. Larger tensile stress was observed in chips with more curl and larger compressive stress was noted in thicker chips. The smaller radius of curvature in a deeper groove tends to produce curlier chips since the chips flowed into the groove and conformed to its geometry. A smaller effective rake

angle tends to produce thicker chips, similar to a small or negative rake angle in flat-faced tool cutting.

5. Reducing the groove width has an overall effect of inhibiting chip upward flow and decreasing the groove curvature. The combined effect produced a thicker and curlier chip, the result of which caused an increase in the compressive and normal stresses.

BIBLIOGRAPHY

[1] Trent, E.M., 1984, *Metal Cutting*, Second Edition, Butterworth & Co. Ltd., London.

[2] Klamecki, B.E., 1973, "Incipient Chip Formation in Metal Cutting — A Three Dimension Finite Element Analysis," Ph.D. Thesis, University of Illinois at Urbana-Champaign, Urbana, IL.

[3] Lajczok, M.R., 1980, "A study of Some Aspects of Metal Machining Using the Finite Element Method," Ph.D. dissertation, NC State University, Raleigh.

[4] Shirakashi, T., Usui, E., 1982, "Mechanics of Machining — From "Descriptive" to "Predictive" Theory," *On the Art of Cutting Metals – 75 Years Later*, ASME Publication PED — Vol. 7, New York, N.Y., pp. 13-35.

[5] Strenkowski, J.S., Carroll, J.T., 1985, "A Finite Element Model of Orthogonal Metal Cutting," *ASME Journal of Engineering for Industry*, Vol. 107, pp. 349-354.

[6] Engelmann, B.E., Hallquist, J.O., 1991, "NIKE2D: A Nonlinear, Implicit, Two-Dimensional Finite Element Code for Solid Mechanics – User Manual," *Lawrence Livermore National Laboratory Report, UCRL-MA-105413.*

[7] Strenkowski, J.S., Carroll, J.T., 1986, "An Orthogonal Metal Cutting Model Based on an Eulerian Finite Element Method," *Manufacturing Processes, Machines and Systems*, Proceedings of the 13th Conference on Production Research and Technology, Society of Manufacturing Engineers, Dearborn, MI, pp. 262-264.

[8] Zienkiewicz, O.C., Godbole, P.N., 1974, "Flow of Plastic and Visco-Plastic Solids with Special Reference to Extrusion and Forming processes," *International Journal for Numerical Methods in Engineering*, Vol. 8, p. 3.

[9] Zienkiewicz, 0.C., Jain, P.C., Onate, E., 1978, "Flow of Solids during Forming and Extrusion: Some Aspects of Numerical Solutions," *International Journal of Solids and Structures*, Vol. 14, p. 15.

[10] Strenkowski, J.S, Moon, K.-J., Oct. 6-9, 1987, "An Improved Finite Element Model of Orthogonal Metal Cutting," *Manufacturing Processes, Systems and Machines*, Proceedings of 14th Conference on Production Research and Technology, Society of Manufacturing Engineers, Dearborn, MI, pp. 67-72.

[11] Shih, A.J.M., Chandrasekar, S., Yang, H.T.Y., 1990, "Finite Element Simulation of Metal Cutting Process with Strain-Rate and Temperature Effects," *Fundamental Issues in Machining*, ASME Publication PED — Vol. 43, New York, N.Y., pp. 11-24.

[12] Komvopoulos, K., Erpenbeck, S.A., 1991, "Finite Element Modeling of Orthogonal Metal Cutting," *ASME Journal of Engineering for Industry*, Vol. 113, pp. 253-267.

[13] Zhang, B., Bagchi, A., 1994, "Finite Element Simulation of Chip Formation and Comparison with Machining Experiment," *ASME Journal of Engineering for Industry*, Vol. 116, pp. 289-297.

[14] Zhang, B., Bagchi, A., 1994, "A Study of Chip Separation and Its Approximation in Finite element Simulation of Continuous chip Formation," *The Physics of Machining Processes - II* , ASME Minerals, Metals & Materials Soc., p. 157.

[15] Shih. A.J., 1995, "Finite Element Simulation of Orthogonal Metal Cutting," *ASME Journal of Engineering for Industry*, Vol. 117, pp. 84-93.

[16] Shih, A.J., 1996, "Finite Element Analysis of The Rake Angle Effects in Orthogonal Metal Cutting," *Int. Jour. Mech. Sci.*, Vol. 38, pp. 1-17.

[17] Huang, J.M., Black, J.T., 1996, "An Evaluation of Chip Separation Criteria for the FEM Simulation of Machining," *Journal of Manufacturing Science and Engineering*, Vol. 118, pp. 545-554.

[18] Wang, B.P., Sadat, A.B., M.J.Twu, "Finite Element Simulation of Orthogonal Cutting — A Survey," *Materials in Manufacturing Processes*, MD-Vol. 8, ASME WAM, Chicago, IL, pp. 97-91.

[19] Bathe, K.-J., *Finite Element Procedures*, Prentice-Hall, Inc., Englewood Cliffs, N.J., 1996.

[20] Hallquist, J.O., Dec. 1986, "NIKE2D – A Vectorized, Implicit finite Deformation finite element Code for Analyzing the Static and Dynamic Response of 2-D Solids," *Lawrence Livermore National Laboratory Report No. UCID-19677*, Rev. 1.

[21] Lin, Z.C., Lin, S.Y., 1992, "A Coupled Finite Element Model of Thermoelastic-Plastic Large Deformation for Orthogonal Cutting," *ASME Journal of Engineering Materials and Technology*, Vol. 114, pp. 218-226.

[22] Whirley, R.G., Engelmann, B.E., 1993, "DYNA3D: A Nonlinear, Explicit, Three-Dimensional Finite Element Code For Solid and Structural Mechanics – User Manual," *Lawrence Livermore National Laboratory Report UCRL-MA-10752.*

[23] Lee, Daeyong, 1984, "The Nature of Chip Formation in Orthogonal Machining," *ASME Journal of Engineering Materials and Technology*, Vol. 109, p.9.

[24] Stephenson, D.A., Agapiou, J.S., *Metal Cutting Theory and Practice*, Marcel Dekker Inc., New York, 1997.

[25] Jawahir, I.S., Zhang, J.P., 1995, "An Analysis Of Chip Curl Development, Chip Deformation and Chip Breaking in Orthogonal Machining," *Transactions of NAMRI/SME*, Vol. XXIII, pp. 109-114.